Journal of Sound and Vibration (2000) **236**(4), 609–621
doi:10.1006/jsvi.2000.2997, available online at http://www.idealibrary.com on IDEAL®

CEPSTRAL PREDICTION ANALYSIS OF THE SIGNAL PATHWAY IN AN ULTRASONIC A-SCAN

M. G. S. Ali and A. Raouf Mohamed

Physics Department, Faculty of Science, Minia University, Egypt

(*Received* 25 *March* 1996, *and in final form* 28 *February* 2000)

Digital deconvolution of ultrasonic echo signals improves resolution and the quality of ultrasonic images. The Homomorphic deconvolution technique under noisy conditions is applied to simulation results in an ultrasonic pulse–echo amplitude scan line. The simulation includes radiation coupling and transducer response, as well as frequency-dependent absorption in the field medium. An accurate method of estimating the pulse-shaping effects of the transducer and the test medium are developed by using Homomorphic filtering. Experimental results are given which confirm the modelling.

1. INTRODUCTION

In order to improve the performance of pulse-echo scanning systems it is necessary to understand the signal path, which consist of transient of diffraction in the acoustic field, ultrasonic absorption and the transducer model. It also requires an approach for detection of the target. System simulation as a precursor to experimental analysis would point to any limitation that may be encountered.

In our simulation, we have considered an unfocused single-element pulse–echo transducer aligned with its face parallel to a lossless target in an absorbing medium. Assuming simple impulse excitation to the transducer, we consider the received echo waveform and its frequency spectrum, at the terminals of the same transducer.

The overall signal path is assumed to be the convolution of four impulse responses representing, respectively, the transducer, acoustic field, absorption and dispersion, and target impulse response. Equivalently, the signal path can be considered in the frequency domain, as a multiplication of the transfer functions representing each of the four phenomena. In the simulation [1, 2] it is possible to take either a time- or a frequency-domain approach for each phenomenon.

Homomorphic filtering [3] is a powerful signal processing method which may be applied to such equivalent one-dimensional models in order to estimate pulse shapes in the medium. The technique has been exhaustively explored in a seismic application [4] and has been tentatively applied to experimental data of ultrasound signals from tissue [5]. Also Hutchins [6] applied Homomorphic filtering for pulse estimation from short-segment echo sequences for normal skeletal muscles.

In this paper, an attempt is made to apply the Homomorphic filtering first to a simulation of the signal formation process in an ultrasonic pulse–echo amplitude scan line in noisy conditions. This is considered necessary since no practical deconvolution process can take place under free-noise conditions. Next experimental system data are used to test the method.

0022-460X/00/390609 + 13 $35.00/0

2. SIMULATION OF THE SIGNAL FORMATION PROCESS

In this paper, the pulse–echo system is viewed as a combination of four physical phenomena: (a) the electric–acoustic properties of the transducer; (b) the non-uniform nature of the acoustic field, as expressed by the radiation coupling response from the transducer to the target and back again; (c) absorption and velocity dispersion, taking typical characteristics of soft biological tissues as an example; (d) target impulse response.

A linear system approach based an input–output description for each phenomena is employed [1, 7]. Each phenomenon is described by a time-domain impulse response or an equivalent frequency domain transfer function. The total system response is obtained by temporal convolution of the subsystem impulse responses or by multiplication of the subsystem transfer functions. A function block diagram of the suggested ultrasonic system model is given in Figure 1.

There are many computer models describing the behaviour of ultrasonic piezoelectric transducers [8–10]. In this paper, the simulation was carried out by using a previously developed digital computer model [1] to evaluate the pulse–echo responses of circular ultrasonic piezoelectric thickness expanders. The model is split into two parts; first, the digital filters are calculated from the basic transfer functions by using mathematical operation routines capable of handling polynomials held in contracted form. Secondly, the sampled time-domain response is obtained by filtering the desired input with the previously calculated digital filters by using an algorithm also capable of handling digital filters supplied in the contracted format. The transducer can be connected to any passive electrical network and furthermore the voltage response at any point in this network can be obtained [11].

Three transfer functions are required for the transducer whose equivalent circuit is depicted in Figure 2. The voltage transfer function, relating the Thevenin equivalent of the excitation voltage V_{ET} to the voltage developed across the transducer terminals (V) can be

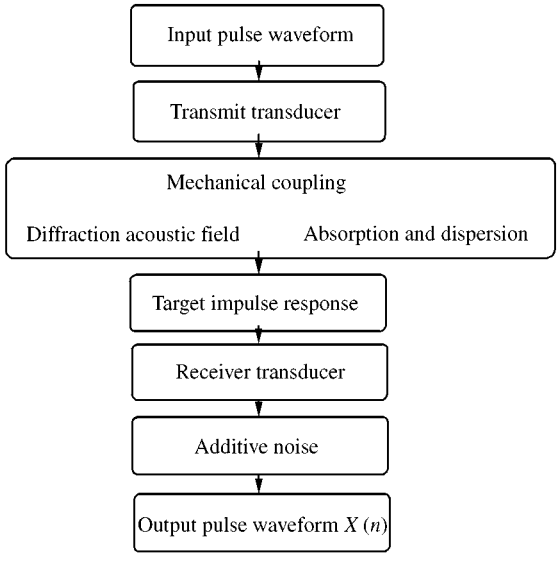

Figure 1. Function block diagram of system model.

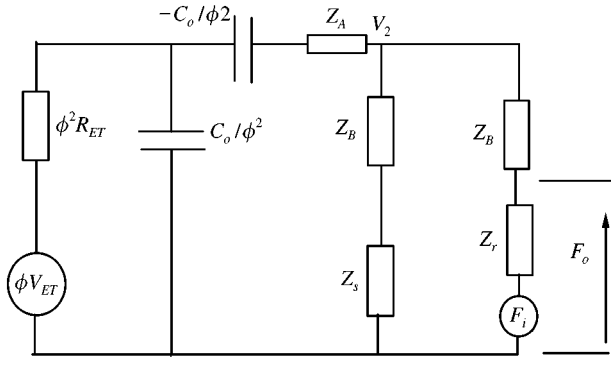

Figure 2. Equivalent circuit of the piezoelectric transducer model.

written as

$$V = \frac{V_{ET}(sC_0R_M - \phi^2)}{sC_0(1 + sC_0R_{ET})R_M - \phi^2}, \tag{1}$$

where

$$R_M = \frac{2Z_AZ_B + Z_B^2 + (Z_A + Z_B)(Z_r + Z_s) + Z_rZ_s}{2Z_B + Z_r + Z_s},$$

C_0 is the static capacitance of the piezoelectric element, and s is the Laplace variable. ϕ represents the electrical to mechanical conversion factor, Z_s and Z_r represent the distributed mechanical impedances at the back and front faces of the piezoelectric element respectively, Z_A and Z_B represent the distributed components of the familiar "T"-equivalent circuit of a transmission line.

The calculation of the transmit and receive transfer functions involves a two-step procedure. For the transmit response, first the response at the point labelled V_2 in Figure 2 is obtained. Next the transmitted force across the matching layers is calculated from the response at V_2 (see reference [12]). On reception, the force transfer across an arbitrary number of matching layers can be written as

$$V = \frac{\{sC_0(1 + sC_0R_{ET})Z_A - \phi^2\}(Z_B + Z_S)F_1}{sC_0(1 + sC_{ET})\{2Z_AZ_B + Z_B^2 + Z_S(Z_A + Z_B)\} - \phi^2(2Z_B + Z_S)}. \tag{2}$$

The Z-transform technique [12] is applied to the Laplace model in Equations (1) and (2) to yield a discrete-time model as a recurrence relationship.

Transient acoustic radiation from circular transducers is most simply formulated in terms of the plane wave–edge wave hypothesis [13]. Starting with the Rayleigh integral pressure at a point in the acoustic field is shown to consist of two components. The first is a plane wave due to axial piston-line movement of the whole active face of the device; this is known as the face wave. It is followed by a diffracted wave emanating from a line source around the periphery of the piston. The two components are of opposite sign and of equal integral in the time domain, yielding zero response at zero frequency.

For a transmission system with two circular transducer aligned coaxially with their faces parallel and upon assuming no energy absorption in the medium between the two devices,

the face wave applies a plane disturbance equally at all points on the receiver. The effect of the edge wave is to sweep across the receiver transducer face, the device response being in proportion to the surface integral of instantaneous pressure on its face. Rhyne [14] extended the fields between a circular transmitter and a point reflector to a signal pathway. The force coupling response by propagation waves for a circular disk transducer in an infinite baffle to a target and back or equivalently a disk to a disk both in infinite baffles has been formulated by Rhyne. Furthermore, Rhyne found the corresponding transfer function in analytical form by Fourier transformation. The solution takes the form of a series expansion, which converges extremely rapidly. The first three terms in this solution are sufficient for the range of geometries considered. Therefore, the solution becomes

$$F(L, a, \omega) = \cos(\omega t_3) + \mathrm{j}\sin(\omega t_3) - \frac{C^2 t_4 t_3}{a^2}\sqrt{\frac{t_4 + t_3}{t_4 + t_1}}.$$

$$\times [\mathrm{J}_0(\omega t_3) + \mathrm{j}\mathrm{J}_1(\omega t_3)] + \frac{C^2 t_2}{a^2}\sqrt{\frac{t_4 + t_2}{t_4 + t_1}}$$

$$\times \left[1 - \frac{t_4}{2(t_4 + t_1)} + \frac{t_4}{2(t_4 + t_2)}\right]\left[\mathrm{J}_0(\omega t_3) - \frac{\mathrm{J}_1(\omega t_3)}{\omega t_3} + \mathrm{j}\mathrm{J}_1(\omega t_3)\right]. \quad (3)$$

Here J_0 and J_1 are Bessel functions of the first kind, C is the wave propagation velocity, j is the imaginary unit, ω the angular frequency, a the transducer radius, t_1 the time of arrival of the face wave, are t_2 corresponds to the furthest distance between points on the periphery of the transmitter and points on the periphery of the receiver. Here, the round trip distance is L and the transducer-target range is $L/2$, $t_1 = L/C$, $t_2 = (L^2 + 4a^2)^{1/2}/C$, $t_3 = (t_2 - t_1)/2$ and $t_4 = (t_1 + t_2)/2$. According to Rhyne, the formulation of equation (3) can be used to represent the radiation coupling transfer function between a disk transducer to a reflector target and back to the same disk transducer. Figure 3 shows the radiation coupling transfer function for a transducer target range of 5 cm.

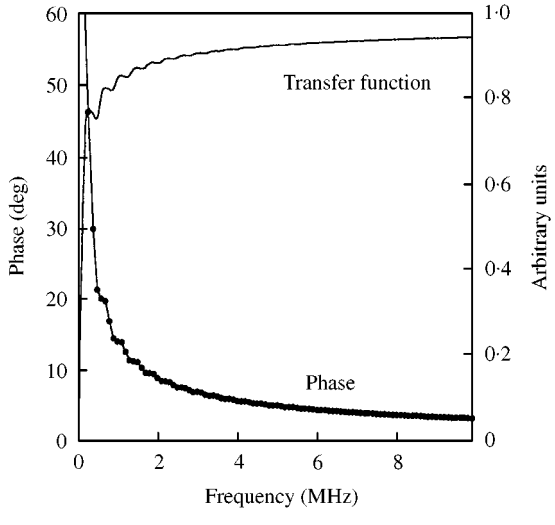

Figure 3. Radiation coupling transfer function in ideal medium as function of frequency.

The influence of attenuation and dispersion in the transmission medium is evaluated by determining the complex wave number K:

$$K(\omega) = \frac{\omega}{C(\omega)} - \mathrm{j}\alpha(\omega) \cdots . \tag{4}$$

Here $C(\omega)$ is the speed of sound in the medium and $\alpha(\omega)$ is the attenuation coefficient. The Kramers–Krong relationship can be used to compute the phase velocity at all frequencies from knowledge of the attenuation coefficient as a function of frequency. Since the magnitude of the dispersion is usually small, it can be approximated by [15]

$$C(\omega) = C_0 + \frac{2C_0^2}{\pi} \int_{\omega_0}^{0} \frac{\alpha(\omega)}{\omega^2} \, \mathrm{d}\omega. \tag{5}$$

where C_0 is the speed of the sound at a reference frequency sound at a reference frequency ω_0. It is well known that the attenuation of ultrasound passing through a lossy medium is frequency dependent [16, 17]. The functional dependence can be modelled either by a power law of the type $\alpha(\omega) = k\omega^n$, where k is constant, and the exponent n generally lies in the range $1 \leqslant n \leqslant 2$. In this work, we have an interest in clinical scanning systems, so we have chosen soft biological tissue as our absorbing medium. The experimentally determined attenuation coefficients for most soft human tissue [18] exhibit an approximately linear relationship with respect to frequency: $\alpha(\omega) = k\omega$. Then

$$C(\omega) = C_0 + \frac{2C_0^2 k}{\pi} \ln\left[\frac{\omega}{\omega_0}\right] \tag{6}$$

and

$$K(\omega) = \frac{\omega}{C_0 + \dfrac{2C_0^2 k}{\pi} \ln\left(\dfrac{\omega}{\omega_0}\right)} - \mathrm{j}\alpha(\omega). \tag{7}$$

The transfer function of the absorption process can be written as

$$T(\omega, L) = \exp[-\mathrm{j}K(\omega)L], \tag{8}$$

where L is the distance from transmitter to target and back again. Equation (8) has been used to simulate the signal path in a scanning system. A function block diagram of the signal formation process is described in Figure 4.

3. DATA SYSTEM EVALUATION

The simulations were carried out by multiplying the transfer functions of the two-transducer responses by the radiation coupling response, transfer function of the transmission medium and the reflector sequence of the target in the frequency domain.

The above simulation was applied using typical transducer data constructed with a lead zirconate titanate (PZT-5A) piezoelectric element [19] with a backing block of tungsten loaded resin [20] and a quarter-wave matching layer of devcon. The transmitter response was obtained for a 10-mm-diameter pulse-echo transducer of 3·5 MHz centre frequency.

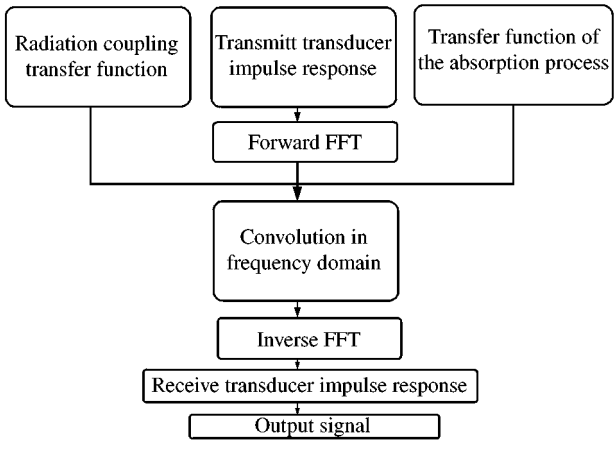

Figure 4. Function block diagram of the signal formation process

TABLE 1

Transducer parameters

Material	PZT-5A
Transducer thickness	6.22×10^{-4} m
Electro-mechanical coupling constant	21.5×10^{8} v/m
Acoustic velocity	4355.0 m/s
Acoustic impedance	$33{\cdot}75 \times 10^{6}$ kg/m^2 s
Thickness of matching layer	$2{\cdot}128 \times 10^{-4}$ m

The transducer parameter are shown in Table 1. The simulations were carried out at an effective sampling time of 5 ns.

In order to investigate the combined effects of the transducer and the phenomena described above on scanning system performance the simulation was applied to a medium of soft biological tissue with an absorption coefficient of 1 dB MHz cm [21]. The reflector sequence of the tissue is shown in Figure 5 corresponding to five-point targets in the tissue. The pulse–echo response of the transducer has been combined with the radiation coupling and medium absorption response for a depth 10 cm in biological tissue. The time-domain response at the receiver terminal is shown in Figure 6. From this figure, it can be seen that the duration of the signal increases after propagation in the lossy medium and the receiver. Figure 7 shows the spectrum of Figure 6. There is a remarkable spectral shift at lower frequencies on the way through the tissue, which results from the frequency-dependent attenuation. The magnitude of spectral downshift in center frequency equal to 500 kHz. The overall time-domain response at the receiver terminal is shown in Figure 8 after being combined with the tissue reflector sequence.

The simulation signal-to-noise ratio values presented here used the average power values for signal and noise in which the average values are obtained by averaging over the time range of interest. The selected value of signal-to-noise level is equal to 25 dB. Figure 9 shows the overall time-domain response at the receiver terminal with signal-to-noise level of 25 dB. The simulated results of Figure 9 will be used in the next section to show the results of the application of the Homomorphic deconvolution technique.

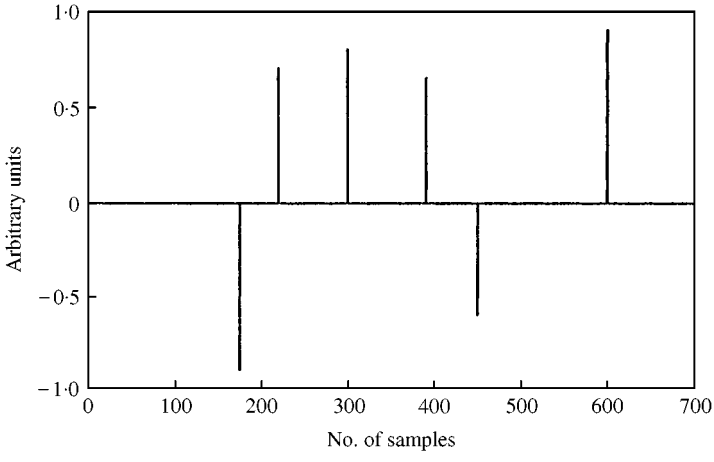

Figure 5. The impulse reflector series of tissue.

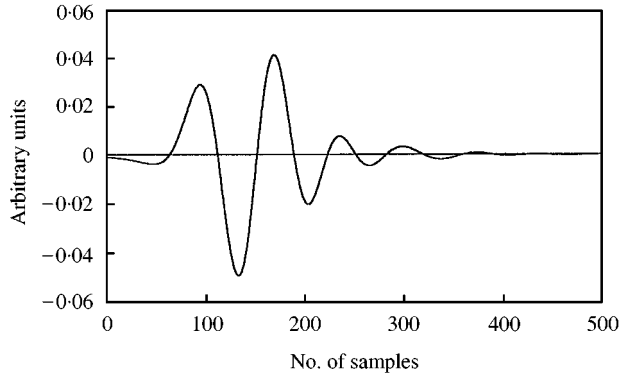

Figure 6. Time-domain simulation for tissue at depth 10 cm.

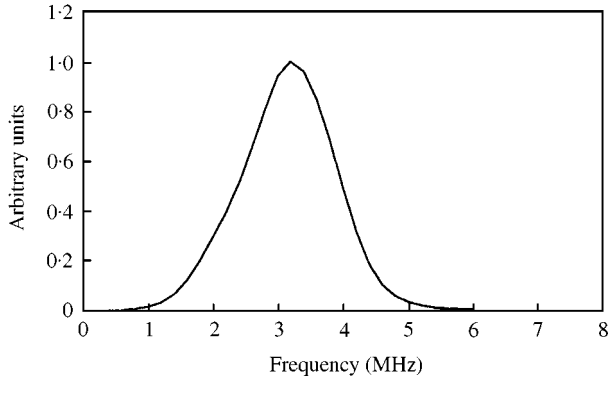

Figure 7. Amplitude frequency spectrum of Figure 6.

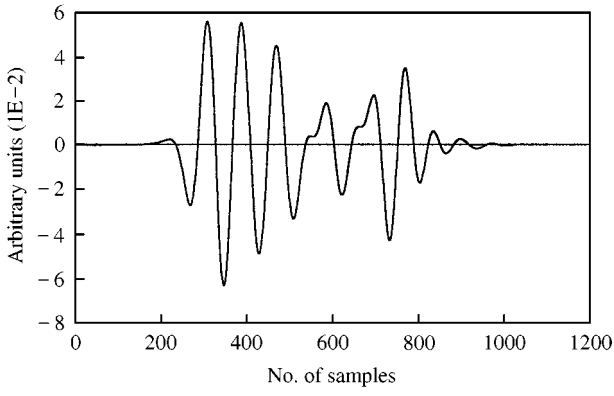

Figure 8. The overall simulation of a pulse–echo 3.5 MHz transducer after propagation 10 cm in soft tissue.

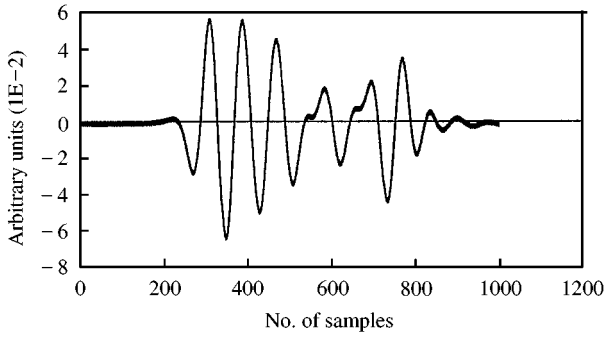

Figure 9. Summation of data of Figure 8 and the Gaussian distribution of random noise at signal-to-noise level 25 dB.

4. HOMOMORPHIC SIGNAL PROCESSING

Homomorphic filtering is a processing method particularly suited to the analysis of convolution-type sequences where echoes are presented. It basically relies on the logarithmic operation, which transforms the produce spectrum of pulse and reflector sequence into an additive one. A further Fourier transformation, into the so-called complex cepstral domain, allows the separation process, between the smooth pulse, and the reflector sequence. The smooth pulse spectrum is concentrated in the low-time region of the cepstral domain, while the reflector spectrum appears in the higher cepstral range. Providing that the two cepstra are indeed separated, then the pulse cepstrum can be isolated by a suitable "low-time lifter", and the pulse recovered by applying the inverse of the operations required to produce the cepstrum.

The technique was devised by Oppenheim [3] and its application to pulse–echo sequences explained in simple fashion by Hutchins [5]. Figure 10 shows the block diagram of the Homomorphic deconvolution technique. In the cepstrum domain, the short-time data are expected to represent the characteristics of the convolving function (impulse response of our composite system). In fact, to recover this component it is recommended to use a short pass window (cepstrum filter or "lifter") of a length (cutoff) equal to approximately one-third of the duration in the impulse response of composite system [22].

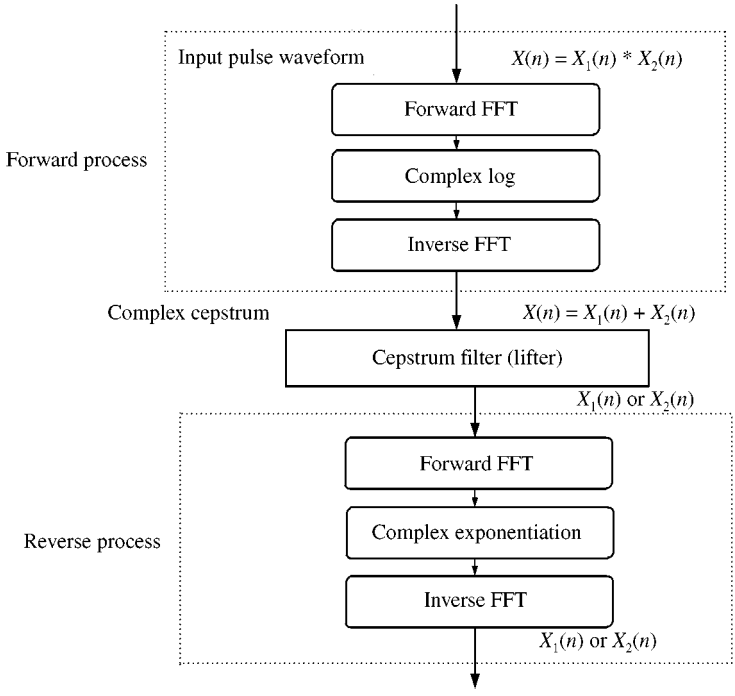

Figure 10. Function block diagram of Homomorphic deconvolution technique.

Figure 11 shows the short time cepstrum of Figure 9. As mentioned previously the impulse response is generally confined to the short time portion of the cepstrum and in this sense it is more "recoverable" than the reflection sequence which has greater spread. Figure 12 and 13 show the short pass and long pass data of Figure 11 obtained by using a rectangular window 50 samples length. It is clear that the effect of the additive noise is visible, because the impulse (reflection) sequence is more sensitive to noise than the impulse response recovery procedure [22]. But, when the signal-to-noise ratio is higher than 33 dB, the reflection sequence is visible as shown in Figure 14. The spectrum of Figure 12 is shown in Figure 15. The spectrum curves in Figures 18 and 15 demonstrate that the Homomorphic deconvolution technique has no effects on the spectrum shift and shape and confirms that Homomorphic filtering is potentially a useful technique for pulse estimation at different depth in the tissues.

5. EXPERIMENTAL METHOD

A modified Sonatest UFD7A scanner was used as the basic data capture instrument. This scanner consists of a broadband pulse generator to excite the transducer and has a variable gain amplifier to amplify the received ultrasound signals. Data recording was achieved by means of a Lecroy 8-bit transient recorder (TR888c) housed in a camac crate (Le Croy 8013). Communication between the transient recorder and the PDP-11/23 computer network was by means of IEEE-488 interface in the camac system (Lecroy 8901) and in one of the computer in the network. The sampling frequency was set to 200 MHz and 1024 data points were recorders for each time-domain signal. The experimental set-up was described by Ali [23].

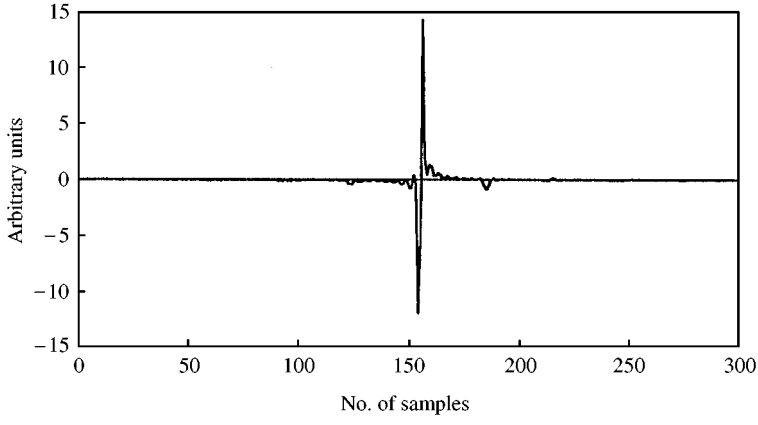

Figure 11. The short time cepstrum of Figure 9.

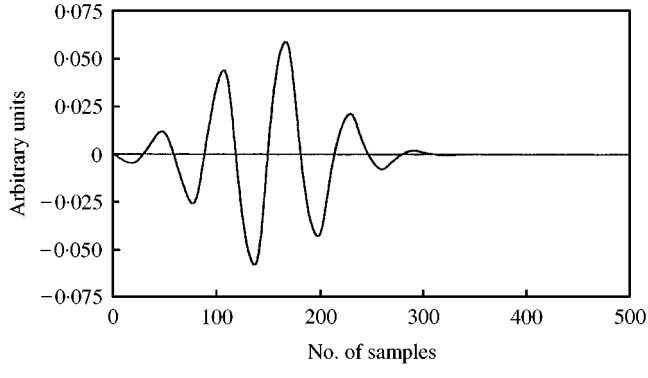

Figure 12. Results of short-pass liftering of Figure 11.

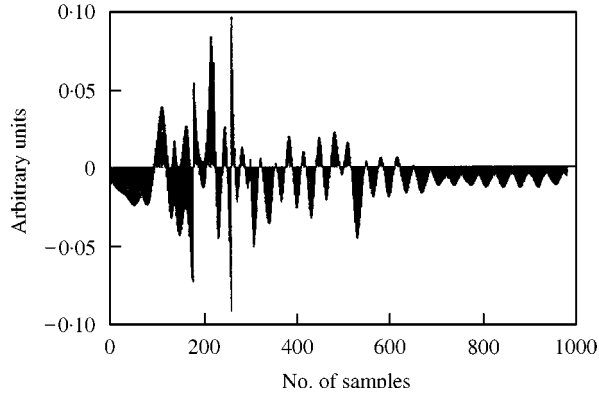

Figure 13. Results of long-pass liftered of Figure 11.

The transducer used in the simulation results will be the same as used in the experiment. The transducer was placed at the top of a castor-oil-filled glass cylinder. The castor oil was used as a test target, because absorption in soft tissue is high and of the same order as absorption in the castor oil. The bottom of the cylinder contained a thick plane reflector

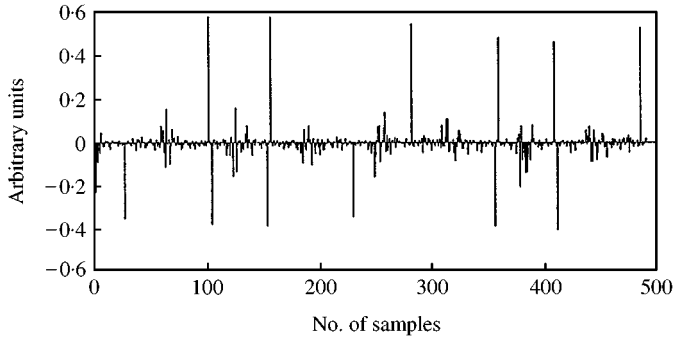

Figure 14. Results of long-pass liftered with signal-to-noise level 32 dB.

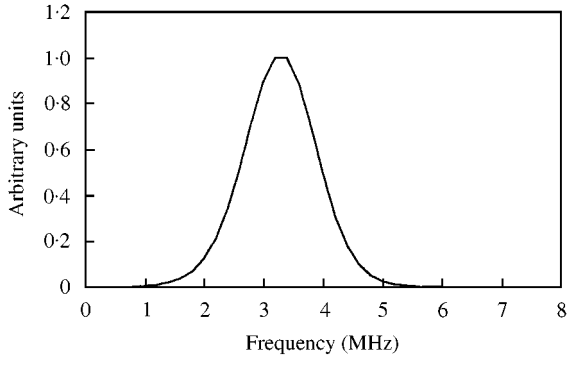

Figure 15. Amplitude spectrum of Figure 12.

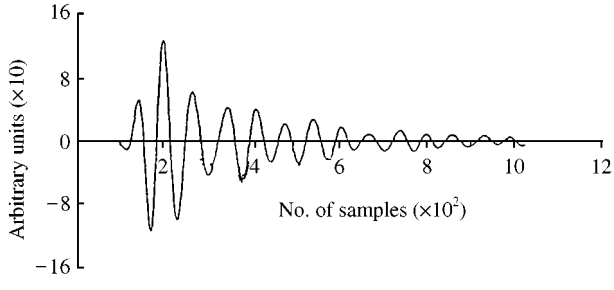

Figure 16. The digitized pulse for medium of castor oil and fine target.

aligned for normal wave incidence. The fine target material (steel wire) was then inserted between the transducer and the reflector. The distance between the transducer and target was 2 cm.

Figure 16 shows the digitized pulse echo for the fine target in castor oil. Because of the delay in the data these exists a high linear phase term, which has to be removed. Figure 17 shows the equivalent long-pass liftered data of Figure 16. It is interesting to note that in the case where the impulse response could be satisfactorily recovered, the reflection sequence is relatively acceptable. The short-pass result for the Figure 16 is depicted in Figure 18.

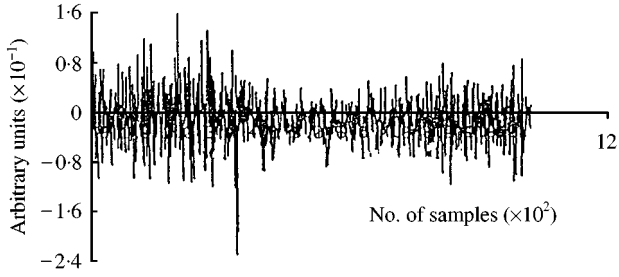

Figure 17. The result of long-pass liftered to Figure 16.

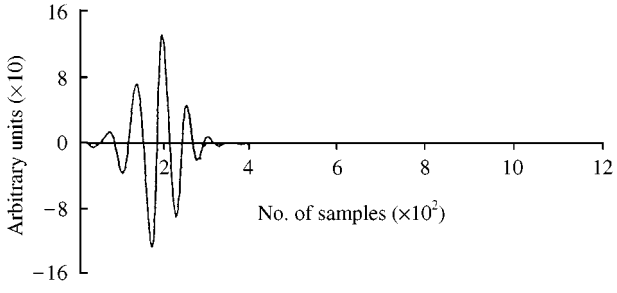

Figure 18. The result of short-pass liftering of Figure 16.

Although in all cases the length of the windowing function in the cepstrum domain was not critical, generally the use of too short a window caused the long-pass data to remain relatively unchanged and the short-pass data to take on a spike-lie appearance. The use of too long a window had also to be avoided, because, as most of the characteristics of the data are confined to the short-time portion of the cepstrum, the procedure would decompose the signal into the whole data length (short-time portion) and a delta function (long-time portion). For all the data, this began to occur for window lengths above approximately 50 samples.

6. CONCLUSION

This paper has described a simple simulation of the signal path in a pulse–echo A-scan system. The model includes the piezoelectric transducer insertion effects, transient radiation coupling process, frequency-dependent absorption in the test medium and the reflection sequence of the target. The computer simulations and experiment presented in this paper all indicate that Homomorphic filtering gives accurate results for estimation of the pulse-shaping effects of the transducer and the test medium. If a signal is the result of linear convolution of a filter with an input (reflection) sequence then the cepstrum processing is a suitable technique to the separation of these two terms. The success of this technique is dependent on the filter function and the input sequence, which occupy different regions in the cepstrum domain. This was found to be the case in the data simulation encountered here.

For the future, it is intended to develop the model further to incorporate a non-linear frequency-dependent attenuating medium. Finally, the model could be extended to measure

the absorption coefficient over a given bandwidth very rapidly and also the result can be used in conjunction with ultrasound pulse–echo imaging systems to partially correct for absorption in the object field. Further work in this direction should, however, develop techniques, which exploit the sparse nature of the reflection sequence.

REFERENCES

1. R. N. Carpenter and P. R. Stepanishen 1984 *Journal of the Acoustical Society of America* **75**, 1084–1091. An improvement in the range resolution of ultrasonic pulse-echo systems by deconvolution.
2. M. G. S. Ali and A. Raouf Mohamed 1995 *Journal of the Acoustical Society of Japan* (E) **16**, 205–211. A simulation packages for the signal pathway in absorbing media under linear perturbation.
3. A. V. Oppenheim and R. W. Schafer 1979 *Digital Signal Processing*. Englewood Cliffs, NJ: Prentice-Hall.
4. J. M. Tribolet 1979 *Seismic Application of Homomorphic Signal Processing*. Englewood Cliffs, NJ: Prentice-Hall.
5. L. Hutchins and S. Leeman 1981 *Ultrasonic International* 81, Z. Novak editor 427–433. Guildford: IPC Press. Pulse estimation from medical ultrasound signals.
6. L. Hutchins and S. Leeman 1982 *Acoustical Imaging* **12**, 459–467. Pulse and impulse response in human tissues.
7. M. G. S. Ali and A. Raouf Mohamed 1992 *Ultrasonic* **30**, 311–316. A simulation of pulse–echo amplitude scan signal formation in absorbing media.
8. E. K. Sitting 1967 *IEEE Transaction of Sonic Ultrasonic* **su-14**, 167–174. Transmission parameters of thickness driven piezoelectric transducers arranged in multilayer configuration.
9. G. K. Lewis 1980 *Acoustical Imaging* **8**, 395–416. A matrix technique for analyzing the performance of multilayer front matched and backed piezoelectric ceramic transducers.
10. G. Hayward, C. J. Macleod and T. S. Durrani 1984 *Journal of the Acoustical Society of America* **76**, 369–382. A system model of the thickness mode piezoelectric transducer.
11. M. G. S. Ali 1997 *Journal of Pure and Applied Ultrasonics* **19**, 85–88. Voltage response at the piezoelectric transducer terminals by Thevinin's theorem.
12. M. G. Ali, 1999 *Journal of Sound and Vibration* **224**, 349–357. Discrete time model of acoustic waves transmitted through layer.
13. P. R. Stepanishen 1971 *Journal of the Acoustical Society of America* **49**, 1629–1638. Transient radiation from piston in an infinite planar baffle.
14. T. L. Rhyne 1977 *Journal of the Acoustical Society of America* **61**, 318–324. Radiation coupling of a disk to a plane and back, or a disk to a disk.
15. M. O'Donnell, E. T. Jaynes and J. G. Niller 1981 *Journal of the Acoustical Society of America* **69**, 696–703. Kramers–Kronig relationship between ultrasonic attenuation and phase velocity.
16. S. Serebian 1967 *Journal of the Acoustical Society of America* **42**, 1057–1063. Influence of attenuation upon the frequency content of a stress wave packet in graphite.
17. J. C. Bamber and C. R. Hill 1981 *Ultrasound in Medicine and Biology* **1**, 121–129. Acoustic properties of normal and cancerous human liver, I. Dependence or pathological conditions.
18. P. N. T. Wells 1975 Ultrasound in Medicine and Biology **1**, 369–387. Review absorption and dispersion of ultrasound in biological tissue.
19. D. A. Berlincourt, D. R. Curran and H. Jaffe 1964 *Physical Acoustics* **1A** W. P. Mason (editor) New York: Academic Press. Piezoelectric and piezomagnetic materials and their function in transducers.
20. M. Redwood 1963 *Journal of Applied Materials Research* **2**, 76–84. A study of waveforms in the generation and detection of short ultrasonic pulses.
21. D. E. Goldmann and T. F. Hueter 1956 *Journal of the Acoustical Society of America* **28**, 35–37. Tabular data of the velocity and absorption of high frequency sound in mammalian tissues.
22. T. J. Ulrych 1971 *Geophysics* **36**, 650–657. Application of Homomorphic deconvolution to seismology.
23. M. G. S. Ali 1989 *Ph.D. Thesis*, *Minia University*, *Egypt*.